Lagrangian simulation of suspended particles in the neutrally stratified surface boundary layer

P. A. Taylor and P. Y. Li
Department of Earth and Atmospheric Science, York University, Toronto, Ontario, Canada

J. D. Wilson
Department of Earth and Atmospheric Sciences, University of Alberta, Edmonton, Alberta, Canada

Received 31 December 2001; revised 11 April 2002; accepted 2 June 2002; published XX Month 2002.

[1] The one-dimensional equation of motion for suspended particles in the neutral atmospheric surface boundary layer is solved for the particle motion assuming that the sequence of vertical fluid velocities at the (moving) particle location can be modeled by a generalized Langevin equation. This inertial particle model is used to produce concentration profiles above a reflecting lower boundary for neutrally buoyant particles with inertia and for heavy particles with gravitational settling. Near the ground, modeled particle number concentration profiles above an infinite plane depart from the standard power law solution predicted by diffusion models. We investigate effective settling velocity and the eddy diffusivity for particles in this turbulent boundary layer flow and find that, near the ground, both are reduced in relation to particle terminal velocity and the assumptions made in boundary layer diffusion models. *INDEX TERMS:* 1863 Hydrology: Snow and ice (1827); 3307 Meteorology and Atmospheric Dynamics: Boundary layer processes; 3379 Meteorology and Atmospheric Dynamics: Turbulence; 4211 Oceanography: General: Benthic boundary layers; 4558 Oceanography: Physical: Sediment transport; *KEYWORDS:* turbulent diffusion, heavy particles, Lagrangian simulation, boundary layers, blowing snow

Citation: Taylor, P. A., P. Y. Li, and J. D. Wilson, Lagrangian simulation of suspended particles in the neutrally stratified surface boundary layer, *J. Geophys. Res.*, *107*(0), XXXX, doi:10.1029/2001JD002049, 2000.

1. Introduction

[2] The classic eddy diffusion scenario for suspended material above an infinite plane source of uniform particles described, for example, by *Prandtl* [1952] assumes a horizontally homogeneous steady (mean) state with upward diffusion ($K_p dN/dz$) balanced by downward settling ($w_s N$) of particles with a uniform settling velocity (w_s), taken positive downward, and with number density $N(\mathrm{m}^{-3})$. If we assume that the eddy diffusivity for particles $K_p = \beta u_* l$ and that the mixing length $l(z) = \kappa(z + z_o)$, then solution of the equation

$$w_s N = \beta u_* \kappa (z + z_o) \frac{dN}{dz} \tag{1}$$

gives the standard power law profile,

$$\frac{N}{N_1} = \left(\frac{z + z_o}{z_1 + z_o} \right)^{-\frac{w_s}{\beta \kappa u_*}}, \tag{2}$$

where N_1 is the number density at some reference height z_1, u_* is the friction velocity, κ is the von Karman constant, and z_o is the roughness length for particle diffusion, here assumed equal to that for momentum. If $z \gg z_o$ or if we measure height starting at z_o, then (2) simplifies to

$$\frac{N}{N_1} = \left(\frac{z}{z_1} \right)^{-\frac{w_s}{\beta \kappa u_*}}. \tag{3}$$

In these equations, β is the ratio of eddy diffusivity for particles (K_p) to eddy viscosity (K_m) (here taken simply as $K_m = u_* l$). Note, however, that the ratio of eddy diffusivity of a passive scalar (K_f) to K_m may also differ from 1.0. Notations vary in the literature but here we use the notation adopted by *Raupach* [2002] with K_m for eddy viscosity, K_f for eddy diffusivity of a passive scalar or "passive fluid element," and K_p as eddy diffusivity for particles. In blowing snow papers, K_s is often used for the eddy diffusivity of snow particles.

[3] There is a major difficulty with the application of (2) or (3) to an infinitely deep layer, since the infinite integral of N with respect to z will only converge for $w_s/\beta\kappa u_* > 1$, and in many cases we expect values of <1. *Kind* [1992] has discussed this for steady state constant flux situations, while *Xiao and Taylor* [2002] investigate this in the context of a time-dependent scenario using an eddy diffusion model.

[4] Particle density distributions are generally observed to satisfy the power law forms above [e.g., *Sommerfeld and*

0148-0227/02/2001JD002049$09.00

Businger, 1965; *Budd*, 1966, *Lees*, 1981, *Shao*, 2000], but we do need to be careful about the specifications of w_s and β. *Businger* [1965] presents a theory for reduction in w_s and values of $\beta > 1$, increasing with $|w_s|/\sigma_w$, where σ_w is the standard deviation of w. We discuss this in section 6.

2. The Inertial Particle Model

[5] We limit our modeling to the neutrally stratified near-surface boundary layer on the basis that blowing snow, sand or dust occurs in high wind speeds and close to the ground so that z/L (where L is the Obukhov length) will be small. Although the focus is on the atmospheric boundary layer, there are many similar situations in the oceans, rivers, or water channels and in industrial applications where there is suspended material in a turbulent, wall-bounded flow. Initial trials were made with a first-order one-dimensional (z) Langevin equation model for fluid element trajectories plus an added gravitational settling velocity for the determination of heavy particle trajectories as utilized by *Wilson* [2000]. However, in the cases of interest for blowing snow or sand, some particles are often close to the ground where the Lagrangian timescale, generally modeled as proportional to z or $(z + z_o)$, is of a magnitude similar to the inertial timescale, defined as mass × velocity/drag. This prompted us to apply an inertial particle or (IP) version of the Lagrangian stochastic model.

[6] In this model we assume that *fluid* velocities in the neighborhood of a particle satisfy a Langevin equation [cf. *Rodean*, 1996]:

$$dw = -\frac{w}{\Gamma_p}dt + \sqrt{\frac{2\sigma_w^2}{\Gamma_p}}d\xi, \tag{4}$$

where $d\xi$ is a Gaussian random increment with zero mean and variance dt. It has units of $t^{1/2}$. The Lagrangian correlation timescale for the fluid velocity along a particle trajectory Γ_p is reduced in relation to that along a fluid trajectory Γ $(= 2\sigma_w^2/(C_o\epsilon))$ by the equation

$$\Gamma_p = \frac{\Gamma}{\sqrt{1 + \left(\frac{\beta' w_g}{\sigma_w}\right)^2}}, \tag{5}$$

following *Csanady* [1963] and *Sawford and Guest* [1991]. In this equation, β' is an empirical, dimensionless constant whose value we set at 1.5 *Wilson* [2000]. We have assumed that σ_w, the standard deviation of w, is independent of z, that the viscous dissipation $\epsilon = u_*^3/l$, with $l = \kappa(z + z_o)$, and that $\sigma_w = bu_*$ (with $b = 1.25$) so that $\Gamma = 2b^3 l/(C_o\sigma_w)$. These are all typical assumptions for the near-surface atmospheric boundary layer and make (4) the uniquely appropriate form for the Langevin equation. The dimensionless coefficient C_o is taken to be 3.125, so that $\Gamma = 0.5(z + z_o)/\sigma_w$, assuming $\kappa = 0.4$ (see section 6 for further discussion of the C_o value). This will be seen later to have consequences for the K_f/K_m ratio, and an adjustment of C_o is needed if we want $K_f = K_m$, at large z.

[7] In the inertial particle model the vertical velocity of a particle (w_p) is governed by the equation

$$\frac{dw_p}{dt} = \frac{w - w_p}{\tau_p} - g', \tag{6}$$

where the first term on the right-hand side represents the aerodynamic drag on the particle, w being the air velocity (vertical) in the vicinity of the particle, and τ_p can be referred to as the particle inertial timescale. This form assumes a linear drag law, appropriate at low Reynolds number, and we can relate τ_p to the settling velocity in still air, w_g, as

$$\tau_p = -\frac{w_g}{g'}, \tag{7}$$

where w_g is negative for consistency with other vertical velocities (in contrast to the standard terminology used, for w_s, in section 1 above). Here $g' = g(\rho_p - \rho)/\rho_p$ is the reduced gravity acting on the particle of density ρ_p in fluid of density ρ. In general, $w_g = -w_s$, but we will retain both notations to distinguish between them, since w_g is specific to still air, while w_s could be based on measurements in a turbulent flow. A basic Lagrangian stochastic (LS) model for fluid elements can be obtained by setting w_g and τ_p to zero and regarding the fluid element as a neutrally buoyant and noninertial particle. In this case, $w_p = w$ and $\Gamma_p = \Gamma$.

[8] We have, for simplicity, adopted a one-dimensional (1-D) approach, ignoring effects of horizontal velocity fluctuations and assuming that the particle instantaneously adjusts its horizontal velocity to that of the surrounding fluid, $U(z)$. Correlations between u and w velocity perturbation may, however, have an effect on particle concentration fields near the surface if upward and downward moving particles have different residence times in a layer. The 1-D approach has another limitation if the particle drag is a nonlinear function of fluid velocity−particle velocity and the present model is restricted to relatively low ($O(1)$) particle Reynolds numbers.

[9] Starting from initial conditions ($t = 0$) for the position and velocity of the particle and of a fluid velocity at the particle position (e.g., $x = 0$, $z = z_{src}$, $u_p = U(z_{src})$, $w_p = 0$, $w = r\sigma_w$, where r is a random number from a Gaussian distribution with zero mean and unit standard deviation), the equations are integrated forward in time over time steps dt to determine new values of x, z, u_p, w, and w_p. Integration in time was forward Euler. The time step Δt was generally taken as $0.05 \times Min\ (\Gamma_p, \tau_p)$. For calculations of trajectories for noninertial particles, with $\tau_p = 0$ as in Figure 1, we set $\Delta t = 0.01\ \Gamma_{p'}$, where $\Gamma_{p'} = Min\ (\Gamma_{p(z)}, \Gamma_{p(0.2\mathrm{m})})$. This is to ensure that time steps are not too large in the upper part of the domain.

[10] Although analytic solution of (6) is possible, within a time step with constant w, and the time step limitation related to τ_p could be relaxed, short time steps are preferred, and it is computationally more efficient to solve (6) by simple finite differences.

[11] Forward integration in time also sets $\Delta x = U(z)\Delta t$ and continues while $x <$ fetch. Treatment of situations where the particle encounters the lower or an upper boundary are discussed in section 4 below.

3. Model Scenario and Background

[12] We first seek to produce a nonevolving concentration profile corresponding to the steady state diffusion model situation as described in section 1 above. To achieve this, we consider the concentration field far downstream of a crosswind line source of particles and assume a reflecting

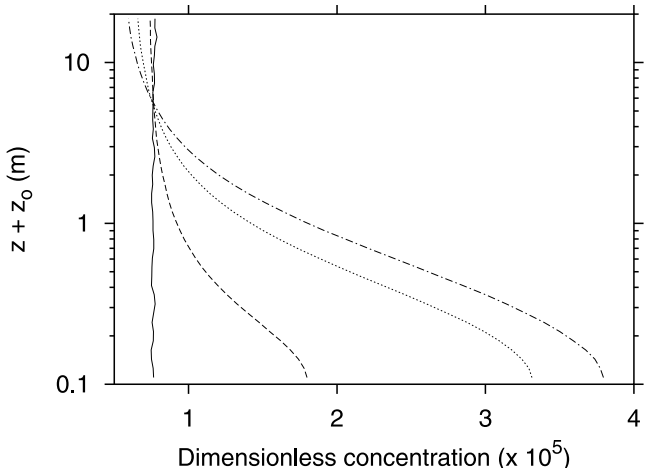

Figure 1. Dimensionless concentration for neutrally buoyant particles. Dashed line, $\tau_p = 0.1$ s; dotted line, $\tau_p = 0.5$ s; dashed-dotted line, $\tau_p = 1$ s; solid line, noninertial, fluid particles, $\Delta t/\Gamma_{p'} = 0.01$.

lower boundary at z_{lb}. In some calculations, z_{lb} is taken at the surface, but it is more efficient to set it above the ground. In view of the difficulty associated with the infinite integral of (2) or (3) discussed in section 1 and to allow the rapid evolution of a statistically steady, nonevolving concentration profile for long fetch, we also utilize an upper reflecting lid for most calculations. Typical runs use 1000 particles, have a 10-km fetch, a lower boundary at 0.01 m or 0.1 m, and often an upper reflecting lid at 20 m. When an upper lid is used, the first particle is released at $z_{src} = 10$ m, with w_p set to zero, and the initial w obtained by using a random number generator. For subsequent particles, initial conditions are taken as the final condition for the previous particle. With no lid, all particles are released from z_{src}. We follow the particle until $x \geq$ fetch and average the concentration for a length denoted by XW. If there is an upper lid, XW is taken as the whole fetch. In the cases when an upper boundary is absent, all particles are treated as first particles and XW is taken as the final 2/3 of the fetch. Particles will typically have "bounced" many times from the lower boundary and, if used, a few times from the upper boundary. The results, with an upper boundary or large enough value of $w_s/\beta\kappa u_*$, can be shown to be independent of source height and fetch, provided the fetch is long enough, and essential features of the concentration profiles are independent of the choice of lower and upper boundary heights.

[13] The concentration profile is determined by computing the total length of time (T_j, #seconds) spent by any of the particles in a window (of height Δz_j, unit width, and length XW) containing the height, z_j, concerned. In order to have similar particle numbers in each window or bin, we use bin sizes that are uniform in ln z rather than z. We place z_j at the logarithmic average height in the window and typically use 40 bins between lower and upper reflection levels. Window height σ_w and time steps need to be selected to avoid particles jumping over a window during a time step. The time step is automatically decreased if this occurs. Within a time step, time is divided proportionally, if necessary, between start and end bins. Averages are based on tracking many (N_p) particles.

[14] The average residence time per particle released per unit (x, z) area is then $T_* = T_j/(N_p \Delta z_j XW)$ (seconds per square meter). We can convert this "residence time" into a dimensionless concentration if we multiply by $u_* \times z_o$, the only velocity and length scales that are common to all of the cases we will consider.

4. Boundary Conditions

[15] The detailed specification of suitable conditions at the lower and sometimes at the upper boundaries is a critical step in the building of a Lagrangian stochastic model for neutrally buoyant particles, as was noted by *Wilson and Flesch* [1993]. It raises even more questions in the case of heavy particles (with nonzero settling velocity) and for our IP model. Reflection at both upper (z_{ub}), and lower (z_{lb}) boundaries prevents any mass flux out of the channel. With just a lower reflecting boundary and unidirectional flow there is still a constant vertically integrated horizontal particle flux, but the layer with particles in suspension may continue to deepen with increasing fetch.

[16] The "real" mechanism by which one might attain an equilibrium profile of heavy, inertial particles must involve a balance of settling out (deposition) and erosion at the surface with zero net vertical flux. While not claiming to fully represent the complex processes that create the near-surface saltation layer, we are hoping to achieve the same overall outcome.

4.1. Neutrally Buoyant Noninertial Particles

[17] If we focus on a lower reflecting boundary, at $z = z_{lb}$, then for neutrally buoyant particles with no inertia ($\tau_p = 0$), i.e., fluid particles, the "smooth wall" assumption usually made in 1-D models is that, at the end of a time step in which the particle trajectory would cross the reflection level, a revised position is given by

$$z = 2z_{lb} - z, \tag{8}$$

and a reversed fluid (and particle) vertical velocity is assumed as the starting value for the next time step, i.e.,

$$w = -w. \tag{9}$$

Provided the time step is sufficiently small and the vertical velocity probability density function (pdf) is Gaussian, this procedure, plus a matching one at an upper boundary, is consistent with the well-mixed condition for noninertial, neutrally buoyant particles in neutral surface layer simulations [*Thomson*, 1987; *Wilson and Flesch*, 1993], in the limit of small time steps.

4.2. Heavy Inertial Particles

[18] For heavy inertial particles ($w_g < 0$, $\tau_p > 0$) we have chosen to reverse w_p at the instant the particles reach z_{lb}, terminate the time step, and compute a new w for the surrounding air. A new time step is then initiated, and the particle is rereleased at z_{lb} with a reversed, positive w_p. The air vertical velocity (w) can be either positive or negative at this point. Different options (reinitialization and w unchanged) were tried for the selection of a w value after the particle has "bounced" from z_{lb} or z_{ub} but $w = -w$ (or

reversal) was considered the most satisfactory (see section 5.5). We will also consider the effect of imperfect elastic rebound of the particles by setting $w_p = -c_r w_p$ at the lower boundary, with c_r acting as a coefficient of restitution.

[19] This reversal condition can also be applied in the case of neutrally buoyant inertial particles ($w_g = 0$, $\tau_p > 0$) and applied at both lower and upper boundaries. Note, however, that inertial particles do not satisfy the "well-mixed" condition, as we will illustrate below.

[20] In the next two sections we present concentration profile predictions and vertical velocity computations for different scenarios. In all cases, we specify surface boundary layer flow and take $u_* = 1$ m s^{-1} and $z_o = 0.003$ m. These are typical values for blowing snow. The equations can be formulated in a nondimensional form based on length (z_o) and time (z_o/u_*) if desired. We use $N_p = 1000$ and a fetch of 10 km for many of these calculations but increase N_p for some cases to obtain stable statistics for large z.

5. Model Predictions

5.1. Neutrally Buoyant Particles

[21] Figure 1 shows concentration profiles for neutrally buoyant particles with reflecting boundaries at $z_{lb} = 0.1$ m and $z_{ub} = 20$ m. The concentration results from noninertial, or fluid, particles confirm that, in the limit of small time step, the model is consistent with the well-mixed condition.

[22] For inertial particles, there are heavier accumulations of particles near the lower boundary and the well-mixed condition is not satisfied. Note that for most aeolian particles τ_p ($= w_s/g'$) is smaller than the values selected here and that the impacts may not be quite as pronounced. The process of accumulation of inertial particles near boundaries in a turbulent flow has been called turbophoresis [*Caporaloni et al.*, 1975; *Reeks*, 1983]. It arises when particles enter regions where their inertial timescales are long in comparison with the local Lagrangian correlation timescale and take a long time to "escape." We cannot rule out the possibility that the reflection strategy has had some influence on the concentration peak near the wall, but we nevertheless do believe the peak is principally due to the mechanism known as turbophoresis.

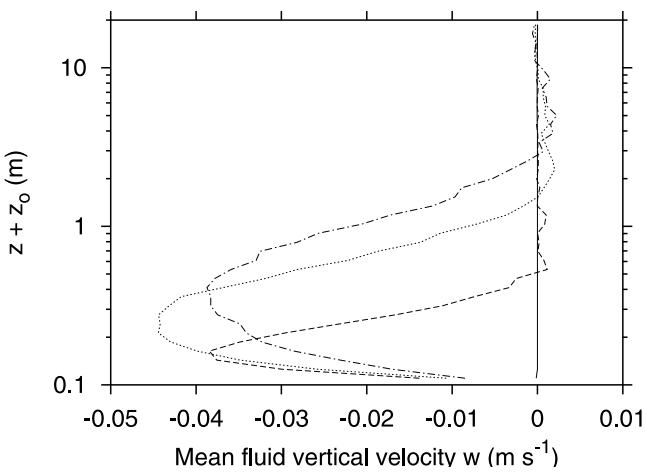

Figure 2a. Mean fluid vertical velocities in the vicinity of inertial, neutrally buoyant particles. Dashed line, $\tau_p = 0.1$ s; dotted line, $\tau_p = 0.5$ s; dashed-dotted line, $\tau_p = 1$ s; solid line, noninertial, fluid particles, $\Delta t/\Gamma_{p'} = 0.01$.

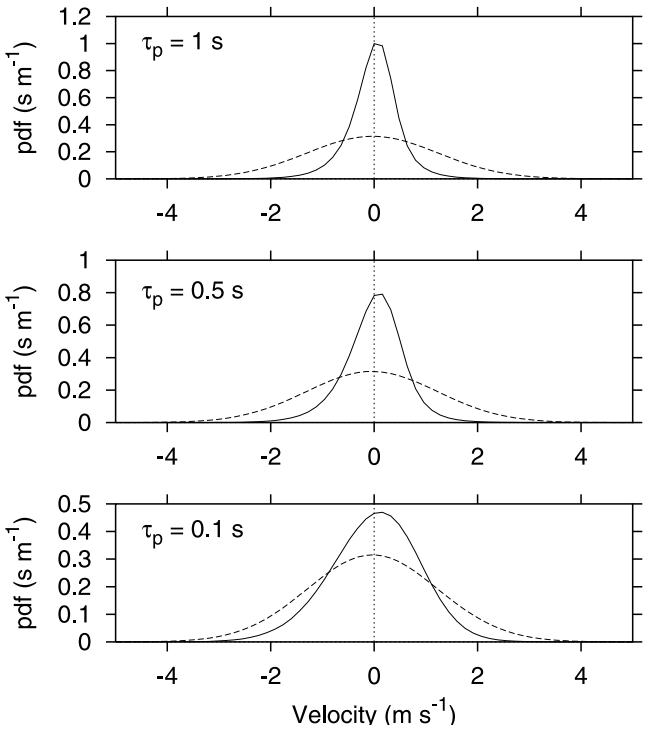

Figure 2b. Velocity probability density functions for inertial, neutrally buoyant particles in the bin centered at $z = 0.2$ m. Solid lines, particles (w_p); dashed lines, fluid in the vicinity of the particles (w).

[23] Figure 2a shows the mean fluid velocities in the vicinity of the neutrally buoyant particles; i.e., these are conditional averages, based on the times when a particle is in a given layer. In order to present smoother velocity distribution profiles, we have increased N_p to 50,000. Corresponding to increased concentrations near the boundary there are negative conditional mean fluid velocities in the region near the wall. The mean vertical component of particle velocity is, however, essentially zero for the three values of τ_p considered here, as expected in steady state conditions. Figure 2b shows the pdfs of vertical velocity for the particles and for fluid in the vicinity of the particles, i.e., w_p and w. Note that the fluid velocity pdfs are essentially Gaussian with a very slight offset to negative values. The particle velocity pdfs are slightly skewed. The effect of inertia is to increase the probability of near-zero w_p values so that inertial particles reside longer at these levels (Figure 2b). As expected, this is more pronounced for the larger τ_p values. The tails for the distributions indicate slightly stronger downward particle velocities than upward, associated, we assume, with the increase of Γ_p with height.

5.2. Heavy Particles: Basic Case

[24] Note first that we will not present results for non inertial heavy particles (i.e., particles for which we might assume $w_p = w - w_g$ at all times), since we have been unable to formulate a satisfactory lower boundary condition for reflection.

[25] As an illustrative case, we set $w_g = -0.5$ m s^{-1} and, as above, place the initial upstream source 10 m above a surface with $z_o = 0.003$ m in a constant stress layer flow with $u_* = 1$ m s^{-1}. We track 1000 particles over the whole 10-km fetch. The lower reflecting boundary is at $z_{lb} = 0.1$ m with a reflecting upper boundary at $z_{ub} = 20$ m when this option is selected. Tests indicated that our choice of Δt was fully satisfactory and confirmed that the results were independent of initial source height. Increasing the number of particles tracked (to 10,000) gave slightly smoother results at the cost of increased computing time. Concentration profiles are shown in Figure 3. With no upper reflecting boundary, some of these particles diffuse to greater height and the corresponding concentrations are thus reduced. With the upper boundary, tests with a longer fetch confirm that an equilibrium has been reached. Extending the fetch to 20 km in the "no top boundary" case does reduce the "equilibrium" concentration profile slightly, but the essential features remain the same.

[26] Away from the lower boundary, the concentration profiles are well described by the power law profile (3). This has a log-log slope of approximately -1.0, corresponding to $\beta = 1.25$ (see later discussion). In the run with a top boundary we can see a slight departure from the power law behavior close to the upper boundary, indicating that our upper reflecting boundary does not accurately represent the unbounded case, which has no such departure.

[27] Confirmation of the power law concentration profile by Lagrangian simulation modeling is a significant feature, but departures from the power law near the ground are of most interest. This appears to be the result of both the lower boundary treatment and turbophoresis in a region where the Lagrangian correlation timescale Γ or Γ_p is comparable to τ_p. In this simulation, $\tau_p \sim 0.05$ s, while Γ ($= 0.5\ (z + z_o)/\sigma_w$) is equal to τ_p at $z \sim 0.13$ m.

[28] Figure 4 shows the mean values of the vertical velocities of the fluid surrounding the particles and of the particles as predicted by our model. These are averages over the times when a particle is in a given height interval (Δz_j).

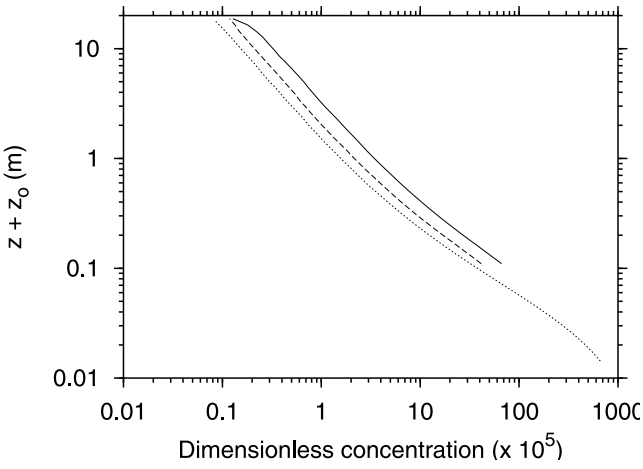

Figure 3. Dimensionless concentration for inertial particles with $w_g = -0.5$ m s^{-1}. Solid line, upper boundary at 20 m and lower boundary at 0.1 m; dashed line, no upper boundary and lower boundary at 0.1 m; dotted line, no upper boundary and lower boundary at 0.01 m.

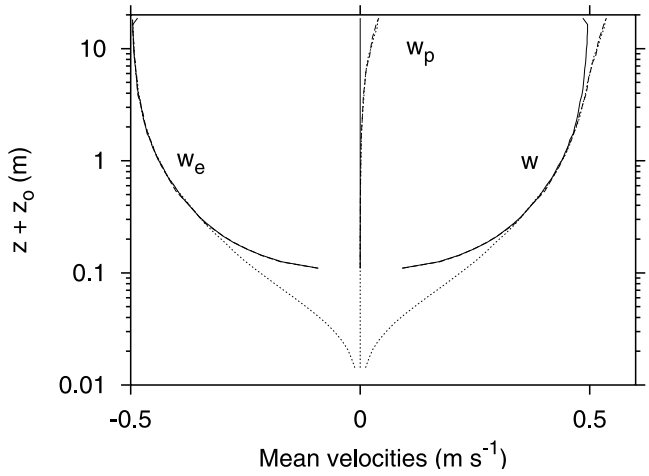

Figure 4. Mean velocities for inertial particles with $w_g = -0.5$ m s^{-1}. Solid line, upper boundary at 20 m and lower boundary at 0.1 m; dashed line, no upper boundary and lower boundary at 0.1 m; dotted line, no upper boundary and lower boundary at 0.01 m.

Results show that the conditional mean fluid vertical velocity increases with height, while the mean particle vertical velocity is essentially zero. The mean particle velocity should be zero if we have a steady, nonevolving profile. The corresponding mean effective (negative) settling velocity ($w_e = w_p - w$) is also shown. In most of the suspension layer, the mean effective settling velocity computed by our model is close to the imposed settling velocity in still air (w_g), but there are departures near the ground which will be significant for moderately large particles.

[29] The reduced settling velocities near the lower boundary are a direct result of the lower boundary condition, modified by effects of turbulence and inertia. By simply reversing w_p at $z = z_{lb}$ we are assuming elastic particles, with a coefficient of restitution, $c_r = 1$. This ensures that the effective settling velocity $w_e = 0$ at z_{lb}. At large heights there is no memory of this "bounce" and $w_e \rightarrow w_g$. The vertical scale over which the transition takes place will depend on the values of w_p at z_{lb} appropriate to particles which will reach a given height, after rebounding from z_{lb}, and the inertial and Lagrangian time scales. If we were simply to ignore the drag on a particle then, if it leaves the surface with a velocity $w_p(z_{lb}) = w_o$, it could reach a maximum height of $z_m = 0.5\ w_o^2/g'$ before gravity turns it back toward the surface. Taking $w_o = -w_g$, $-w_g + \sigma_w$ and $-w_g + 2\sigma_w$ would give $z_m \approx 0.013$, 0.16, and 0.45 m, respectively with the values assumed for Figure 4 ($w_g = -0.5$ m s^{-1}, $\sigma_w = 1.25$ m s^{-1}) and with $g' = 9.81$ m s^{-1}. These are consistent with the height variation of w_e. The respective corresponding travel times (surface to z_m, $t = w_o/g'$) are approximately 0.05, 0.18, and 0.3 s, respectively, and 0.05 s is also the inertial timescale ($-w_g/g'$). Note that the Lagrangian timescale for the particles (7) is reduced slightly from that of the air, but the air values ($\Gamma = 0.5(z + z_o)/\sigma_w$) are comparable to the travel times for the higher-velocity particles, in partial support of our "no-drag" estimates.

[30] Noting that $-w_e < -w_g$, we could potentially revisit the Γ_p calculation (7). In the basic case ($\sigma_w = 1.25$ m s^{-1}, $w_g =$

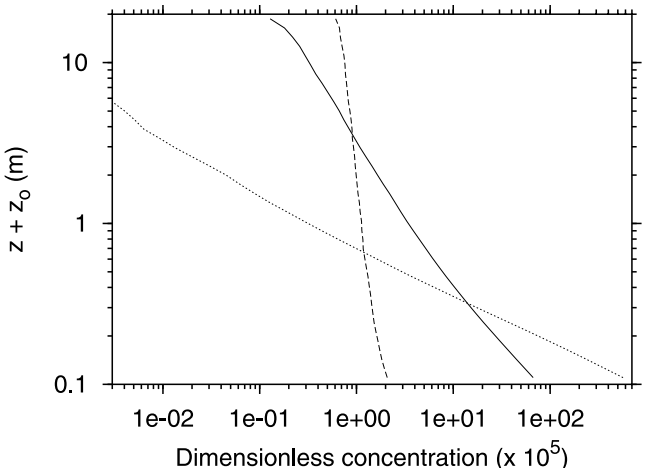

Figure 5a. Dimensionless concentration for inertial particles. Dashed line, $w_g = -0.1$ m s^{-1}; solid line, $w_g = -0.5$ m s^{-1}; dotted line, $w_g = -1$ m s^{-1} and $z_{ub} = 20$ m.

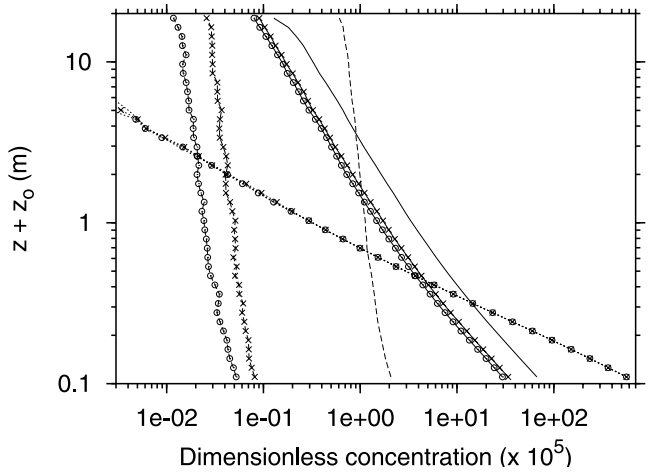

Figure 5b. Dimensionless concentration for inertial particles without a top boundary. Lines are for 10-km fetch; symbols are for results obtained over different fetch ranges within a 60-km fetch. Dashed line, $w_g = -0.1$ m s^{-1}; solid line, $w_g = -0.5$ m s^{-1}; dotted line, $w_g = -1$ m s^{-1}. Crosses, averaged over 20 to 30 km; circles, averaged over 50 to 60 km.

-0.5 m s^{-1}), however, the ratio $\Gamma_p/\Gamma = 0.86$, and an iterative approach to this adjustment did not seem warranted.

5.3. Sensitivity Tests

[31] We have altered the lower boundary and top boundary heights and examined their effects on the model results. All concentration profiles have similar features, and the slopes in the suspension layer are in close agreement. Optimum results have no upper boundary. Reducing z_{lb} leads to reduced time steps and increased computer time, but (Figures 3 and 4) the results match those with $z_{lb} = 0.1$ m. Nonzero particle vertical velocities for large z (Figure 4) and the existence of a positive vertical mass flux indicates that in cases with no upper boundary, equilibrium has not quite been reached for this fetch at all heights.

5.4. Results With Different Settling Velocities

[32] Concentration profile predictions for particles with $w_g = -0.1$, -0.5, and -1.0 m s^{-1} are shown in Figure 5a. All other physical parameters prescribed here are the same as in the typical scenario and we use $z_{ub} = 20$ m. As in our basic case, these are approximately equivalent to the power law solutions (3), with slopes varying with w_g.

[33] The mean particle vertical velocities (not shown) for all three values of w_g considered here are very close to zero, indicating that a near steady state has been reached. We notice in Figure 5a that the obvious effect of larger values of settling velocity is to cause heavier accumulation of particles close to the lower boundary.

[34] As was noted by *Xiao and Taylor* [2002], particles with $-w_g/(\beta\kappa u_*) < 1$ may not reach an equilibrium state. With our values of β (see section 6) and u_* and with no upper boundary, there would be no equilibrium in the cases with $w_g = -0.1$ and -0.5 m s^{-1}. To verify their conclusion, we remove the upper boundary in our model and compare our model results for the standard fetch (i.e., 10 km) with those for 60-km fetch. Concentration results are obtained over different fetch ranges. The concentration profiles of particles are shown in Figure 5b. Note that we only show the concentration profile as high as 20 m. The concentration profiles for longer fetches are shifted lower in the "no upper boundary" case. This is due to the fact that when there is no lid, suspended particles can be carried by the turbulent airflow to greater heights, resulting in smaller particle concentration at each level of the computational domain. The shape and slope of the concentration profiles are, however, the same, and for $w_g = -1$ m s^{-1} the results are essentially identical.

[35] Calculations of effective settling velocities, with and without an upper reflecting boundary, gave very similar results. Figure 6 shows results for the ratio of w_e/w_g for our three cases with $u_* = 1$ m s^{-1}. We can note that for $u_* = 1$ m s^{-1} the depth of the region with reduced settling velocity is greater with $w_g = -1$ m s^{-1}. Cases with fixed w_g (-0.5 m s^{-1}) and varying u_* indicate that larger values of u_*, and thus of σ_w, also increase the depth of the region.

5.5. Results With Different Lower Boundary Treatments

[36] As was noted above in section 4.2, our standard treatment of inertial particles encountering the lower boundary is to restart them with both w and w_p reversed. We have

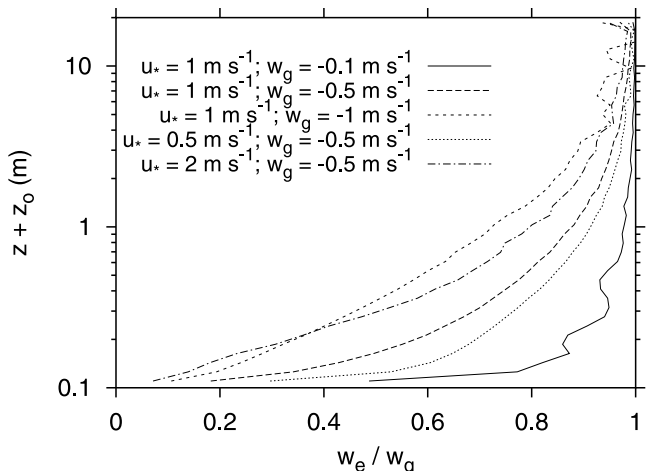

Figure 6. Comparison of ratio of particle effective settling velocity to terminal velocity; $z_{lb} = 0.1$ m.

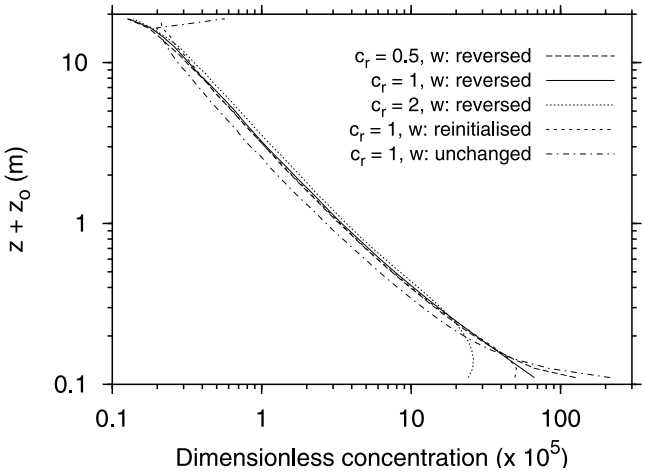

Figure 7a. Comparison of dimensionless concentration for inertial particles with $w_g = -0.5$ m s^{-1} and various boundary conditions.

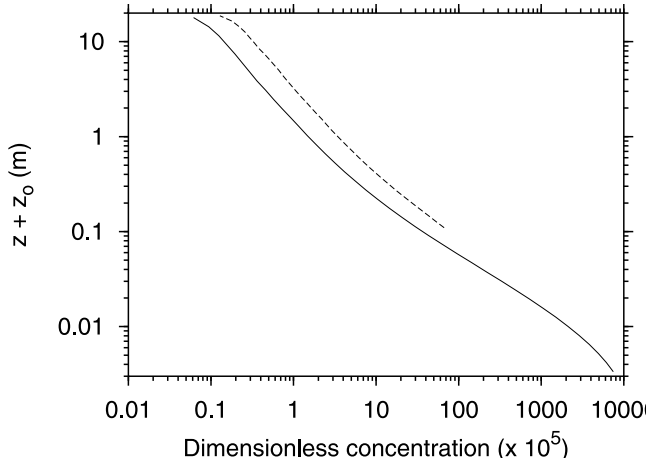

Figure 8a. Dimensionless concentration for inertial particles with $w_g = -0.5$ m s^{-1}. Dashed line, $z_{lb} = 0.1$ m; solid line, $z_{lb} = 0$ m and $z_{ub} = 20$ m.

also made calculations with w unchanged or reinitialized and with $w_p = -c_r w_p$, where c_r is a coefficient of restitution different from 1.0.

[37] When we change our treatment of w at both the lower and upper boundaries, the concentration profiles show departures from the power law form close to these boundaries but retain the same form in between, as shown in Figure 7a. In the case with w reinitialized, the particle concentration is reduced slightly near the lower boundary but increased slightly near the top boundary. With w unchanged, the particle concentrations near the boundaries are increased, with corresponding but slight reductions in between.

[38] The engineering literature on two-phase flows generally deals with smaller-scale, smooth wall situations but has considered both elastic and inelastic particles [e.g., *Devenish et al.*, 1999]. To illustrate the impact of different values of the coefficient of restitution in our model, we have made calculations with $c_r = 0.5$ and $c_r = 2.0$ (an ejection mode). Concentration profiles are included in Figure 7a. We notice that with the increase of c_r, the particle concentration near the lower boundary decreases, while the particle concentration in the suspension layer increases (very slightly). This is expected, since the larger the value of c_r, the larger the value of w_p after reflection and hence the higher a particle can jump from the lower boundary.

[39] Figure 7b shows the mean velocities with the three values of c_r. The impact of c_r on w_e is clearly observed close to the lower boundary, but the values for large z are essentially unchanged. With $c_r = 2$, we can see from Figure 7b that there is negative mean w (and hence positive mean w_e) in the region just above the bottom surface, corresponding to the layer with $dN/dz > 0$ in Figure 7a.

5.6. Results With $z_{lb} = 0$ m

[40] In this section we present some model results with the lower boundary at $z = 0$. Figure 8a shows the concentration profiles with $w_g = -0.5$ m s^{-1} using $z + z_o$ as the ordinate. The result with $z_{lb} = 0.1$ m is also shown for comparison. In this figure, we observe a heavy accumulation of particles as the ground is approached, relative to downward extrapolation of the power law profile, which we believe is again a manifestation of turbophoresis. Vertical

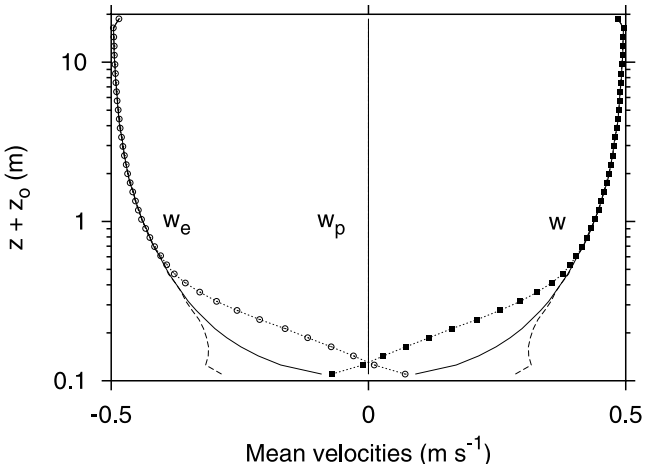

Figure 7b. Mean velocities for inertial particles with $w_g = -0.5$ m s^{-1}. Dashed line, $c_r = 0.5$; solid line: $c_r = 1$; dotted line with circles or squares, $c_r = 2$.

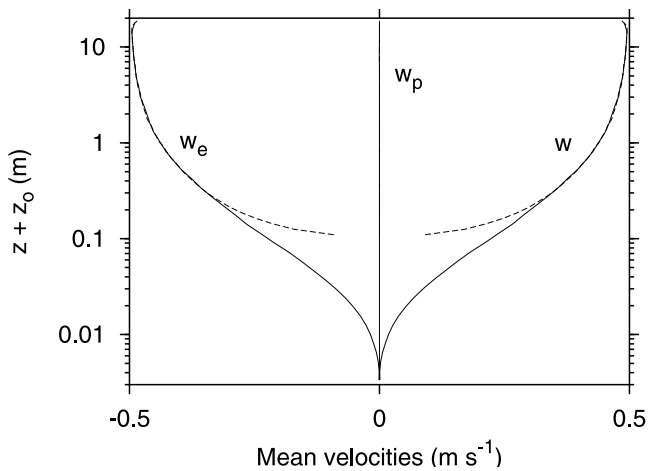

Figure 8b. Mean velocities for inertial particles with $w_g = -0.5$ m s^{-1}. Dashed line, $z_{lb} = 0.1$ m; solid line, $z_{lb} = 0$ m.

Table 1. Particle Trajectory Length Between Bounces at the Lower Boundary (*LB*) and Upper Boundary (*UB*)[a]

	z_{lb} = 0 m		z_{lb} = 0.01 m		z_{lb} = 0.1 m	
w_g, m s^{-1}	at *LB*	at *UB*	at *LB*	at *UB*	at *LB*	at *UB*
−0.1			175.7	981.4	320.7	974.7
−0.5	0.4	9708.7	1.8	7142.9	12.9	4132.2
−1			0.3		1.9	

[a] Particle trajectory length is in meters; z_{ub} = 20 m, N_p = 1000, and z_o = 0.003 m.

velocity profiles are shown in Figure 8b. It is clear in Figure 8b that they are all essentially zero at the ground. The run with $z_{lb} = 0$ takes significantly more computer time but indicates that it is acceptable to use $z_{lb} > 0$.

5.7. Particle Trajectories

[41] Particle trajectory lengths between bounces can be computed by dividing the fetch by the average number of bounces made by the N_p particles at the lower (or upper) surface. Table 1 shows the results from our IP model for different values of w_g and z_{lb} with z_{ub} = 20 m and N_p = 1000. It is quite clear from Table 1 that at the lower boundary, the length between bounces increases with the increase of z_{lb} and decreases with the increase of $|w_g|$. The situation is the opposite at the upper boundary; i.e., the length between bounces decreases with the increase of z_{lb} and increases with the increase of $|w_g|$ Note that the lengths between bounces at the top boundary for $w_g = -1$ m s^{-1} are not shown because the average number of bounces for the cases considered here is less than 1 over the entire fetch.

6. Comparisons With Businger's Theory

[42] *Sommerfeld and Businger* [1965] reported on measurements of blowing snow in the Arctic. Their analysis suggested that the eddy diffusivity for blowing snow (K_p) is almost an order of magnitude larger than the eddy diffusivity for passive scalars (K_f, assumed equal to K_m), in contrast to the theory presented by *Csanady* [1963] indicating a reduced value. Subsequently, *Businger* [1965] developed an essentially Eulerian theory to explain why this ratio could be so large and also addressed the impacts of inertia on settling velocities. Our LS model results are generally in conflict with Businger's theory.

[43] When considering settling velocity, Businger used a nonlinear drag formula (drag proportional to $(w_p - w)^{1.75}$), assuming particles of diameter d = 2000 μm, and a settling velocity of 1.5 m s^{-1}, giving a Reynolds number of approximately 250 (kinematic viscosity, $\nu = 1.2 \times 10^{-5}$ m^2 s^{-1}). In this range a nonlinear drag formulation is appropriate, but for more typical blowing snow or ice particles (d = 50 μm, w_s = 0.25 m s^{-1}), $R \approx 1$ and a linear drag law, as has been applied here, can be used. For relatively large, fast moving particles with $R > 1$ it would be quite feasible to introduce a nonlinear drag into a 3-D IP model, but we have not so far implemented this.

[44] Businger's discussion is based on the motion of an inertial heavy particle subject to sinusoidal fluctuations in the vertical velocity of the surrounding air, w. The essence of his argument is that the drag on a falling particle is greater for positive w than for negative w, since the relative velocities are greater. Nonlinearity in the drag law then leads to an average drag that is greater than that experienced by a particle falling at the same speed in still air. With a linear drag law this does not apply, and the reduced settling velocity computed by our model has a totally different mechanism, as was discussed above in section 5.2. *Businger* [1965, p. 3308] claims that, "for settling speeds greater than 1 m s^{-1} and (10 m) wind speeds <20 m s^{-1}, the reduction of average settling speeds by turbulence is negligible." His computations do, however, show reductions of the order of 35% for particles with w_s = 0.5 m s^{-1} at a height of 0.5 m in a wind of 20 m s^{-1}. This could be considered as significant and happens to be reasonably close to our own result (Figure 6), where a 23% reduction is predicted when u_* = 1 m s^{-1} ($U_{10\ m}$ = 20.3 m s^{-1} with z_o = 0.003 m). In both cases, w_e/w_g increases (i.e., the effect is reduced) with increasing height, as can be seen in Figure 6. For a specified height, Businger's theory (see his Figure 1) and our model (Figure 6) have w_e/w_g reducing (increased effect) with increasing velocity or u_* for a particle with a given w_g, but for fixed u_* and height, our model shows an increasing effect (i.e., w_e/w_g is reduced) with increasing w_g, while Businger's results have w_e/w_g increasing. In Businger's model, more inertia (increased w_g) makes turbulent drag fluctuations less important, relatively, while in our case, more inertia will lead to a higher bounce.

[45] Businger's theory for an increase in the eddy diffusivity of particles is based on the notions that the net flux of particles through a given level should be zero and the fractional horizontal cross-sectional area containing upward moving particles (α) should be smaller than the fraction (1 − α) containing particles moving downward. It also assumes $w_p = w + w_g$ and a Gaussian distribution with zero mean for the vertical component of air velocity, w. In Eulerian continuum terms this leads to higher air particle concentrations or densities in upward than in downward moving particle parcels; and in addition, the average upward velocities in these parcels will be stronger (in absolute value) than the downward ones. Coupled to assumptions concerning the air particle concentrations in upward and downward moving particle areas and a mixing length assumption, Businger obtains significant increases in the ratio K_p/K_m as a function of $-w_g/\sigma_w$. The ratio appears to be independent of height. For our basic case ($w_g = -0.5$ m s^{-1}, $u_* = 1.0$ m s^{-1}), $-w_g/\sigma_w = 0.4$ and $K_p/K_m \approx 1.14$, while with $w_g = -1.0$ m s^{-1}, $-w_g/\sigma_w = 0.8$ and $K_p/K_m \approx 1.71$, extracting values as best we could from Businger's Figure 4. Significantly higher values (about 10 for $-w_g/\sigma_w = 3$) are obtained for faster settling particles, but in our view, these scenarios are less realistic, since very few particles of this nature would be airborne.

[46] Within our Lagrangian model the vertical velocity distributions of both the particles and the surrounding air are essentially Gaussian, with zero mean for the particles but a mean value of $-w_e$ for the air (Figure 9). Note that the fluid velocity distributions are essentially the same at all heights and correspond to a Gaussian distribution with σ_w = 1.25 m s^{-1}. They do, however, have a nonzero mean, since they are conditionally sampled only when a particle is in the layer that they are based upon. The particle vertical velocity pdfs are approximately Gaussian with zero mean, but as the lower boundary is approached, σ_{wp} decreases and the pdf

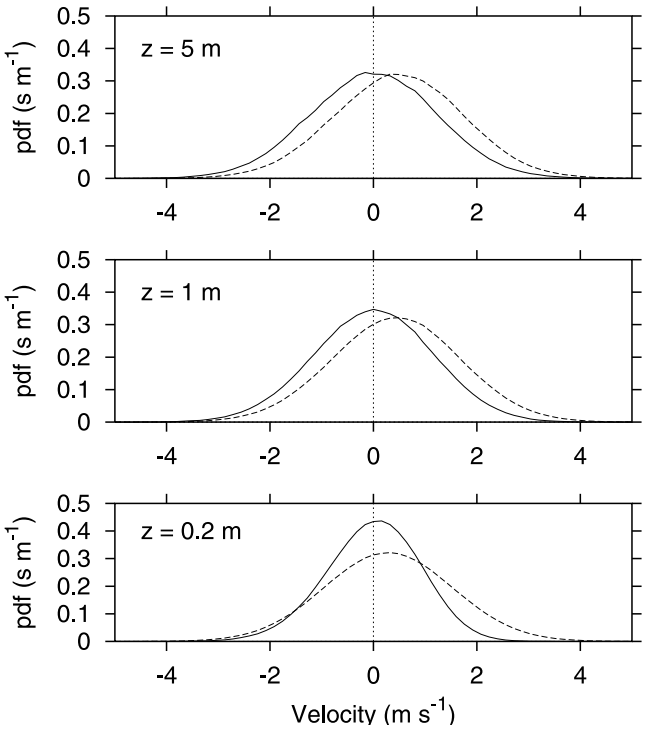

Figure 9. Probability density function of velocities for IP model with $w_g = -0.5$ m s^{-1}. Solid lines, particle vertical velocity (w_p); dashed lines, fluid vertical velocity (w).

becomes narrower and slightly skewed. As with the value of w_e, this is a result of particles "bouncing" from the lower boundary. At low heights some particles are near the top of their trajectories after bouncing off the lower boundary, and there will be an increase in the likelihood of near-zero values for w_p. At larger distances from the ground, $\Gamma \gg \tau_p$ and fluid and particle vertical velocity pdfs are simply offset by w_g, as in Businger's model.

[47] A direct calculation of K_p and $\beta = (K_p/K_m)$ can be made from the concentration and profiles determined from the IP model results if we assume that there is a balance between upward diffusion and downward settling as in (1). In terms of $\ln(z + z_o)$ we have

$$-w_e N = \beta u_* \kappa \frac{dN}{d\ \ln(z + z_o)}$$

or

$$\beta = -\frac{w_e}{u_* \kappa} \frac{d\ \ln(z + z_o)}{d\ \ln(N)},$$

where β can be a function of z. We can approximate $d \ln(z + z_o)/d \ln(N)$ by a central finite scheme in the plot of $\ln N$ versus $\ln(z + z_o)$, and the values of β then computed are shown in Figure 10a.

[48] First-order Lagrangian stochastic models imply an underlying diffusivity for fluid elements, as was noted by *Wilson and Sawford* [1996]. The "diffusion limit" of an LS model was examined formally by *Durbin* [1984] and by *Sawford and Guest* [1988]. It is known that the effective diffusivity implied by the specific LS model (4) is

$$K_f = \sigma_w^2 \Gamma,$$

and with $\Gamma = 2\sigma_w^2/(C_o \epsilon)$ it follows that

$$\frac{K_f}{K_m} = 2\frac{b^4}{C_o} = 1.56,$$

where $b = \sigma_w/u_*$ is taken equal to 1.25 and we have used *Wilson*'s [2000] value of 3.1 for C_o. The "diffusion limit" of 1.56 is plotted in Figure 10a in comparison with the ratios K_p/K_m. However, the 1.56 value is for fluid particles (neutral buoyancy, no inertia, so the ratio applies to K_f/K_m). This can be reduced for heavy particles according to the ratio $K_p/K_f = \Gamma_p/\Gamma$ and leads to limiting values of $K_p/K_m = 1.55$, 1.34, and 1.00 for the 0.1, 0.5, and 1.0 m s^{-1} settling velocities, respectively, used here. These are in general agreement with the ratios extracted from the number density profiles, although they are noisy and there are departures near the upper boundary, which we attribute to the upper reflecting boundary. There are also departures near the upper boundary, which we attribute to the upper reflecting boundary. Note that in Figure 10a we have not shown results for $z > 1$ m in the $w_g = -1$ m s^{-1} case, since few such particles get above that level and the statistics are not reliable. It is, however, very clear that β is a function of z and that β is reduced significantly as we approach the lower boundary; indeed $\beta \to 0$ as $z \to 0$.

[49] The specification of C_o and the related K_f/K_m ratio in the diffusion limit are somewhat controversial. *Sawford*'s [2001] comparisons of concentration profiles from Lagrangian simulations with data from Project Prairie Grass confirm the findings of *Wilson et al.* [1981] $K_f/K_m > 1$ and generally support our choice of C_o value. However, as *Sawford* [2001, pp. 175–178] notes "These findings clearly need to be tested against other data sets." Note that our main findings and conclusions are not dependent on the C_o value used, as has been confirmed with computations with

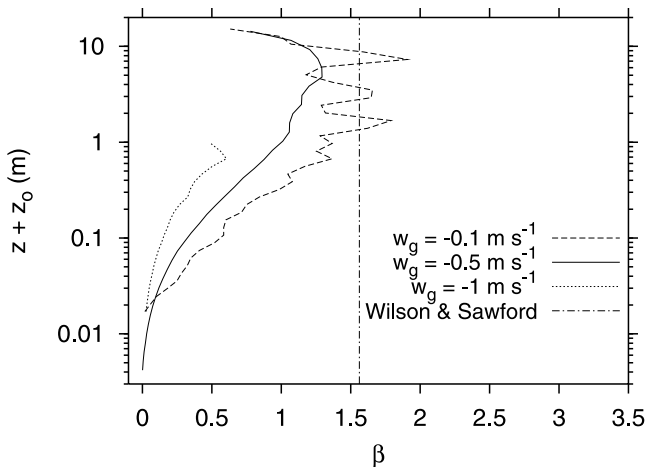

Figure 10a. Ratio of eddy diffusivity to eddy viscosity, β, for different values of w_g with 1000 particles; $z_{ub} = 20$ m, $z_{lb} = 0.01$ m with $w_g = -0.1$ and -1 m s^{-1}, and $z_{lb} = 0$ m with $w_g = -0.5$ m s^{-1}.

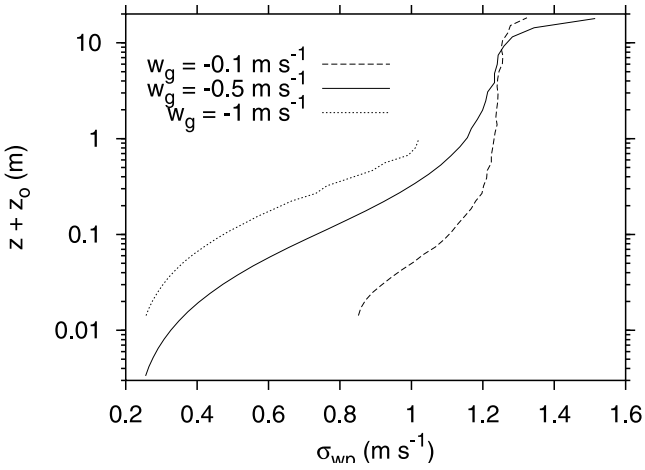

Figure 10b. Height versus σ_{wp} for different values of w_g with 1000 particles; $z_{ub} = 20$ m, $z_{lb} = 0.01$ m with $w_g = -0.1$ and -1 m s^{-1}, $z_{lb} = 0$ m with $w_g = -0.5$ m s^{-1}.

$C_o = 4.88$ for which $K_f/K_m = 1.0$. In both cases, the assumptions related to the reduced Lagrangian timescale for particles lead to $K_p/K_f < 1$ in the diffusion limit as noted by *Raupach* [2002].

[50] If we think of an eddy diffusivity as a product of a velocity scale (σ_{wp}) and a mixing length, associated with a "mean free path" of the particle, we would expect reductions in both of these, relative to σ_w and κz, as a result of particle inertia. Computations of (σ_{wp}) are shown in Figure 10b. For the case with $w_g = -0.5$ m s^{-1}, $u_* = 1$ m s^{-1} a smooth reduction is clearly observed with (σ_{wp}) reducing from 1.25 m s^{-1} ($1.25u_*$) for large z to about 0.3 m s^{-1} as $z \rightarrow 0$. Reductions for particles with $w_g = -1$ m s^{-1} are even more pronounced.

[51] The puzzle in some ways is to reconcile $\sigma_{wp} \neq 0$ with β (and thus K_p) $\rightarrow 0$ as $z \rightarrow 0$. Since $w_e = 0$, because of our boundary condition, and noting that $dN/dz \neq 0$ as $z \rightarrow 0$, we need $K_p = 0$ to achieve a zero diffusive flux at the surface (where $K_m = \kappa u_* z_o$) in order to balance the zero settling flux ($w_e N$). The answer may simply be that flux-gradient relationships should not be used in this region close to a wall where the inertial timescale is larger than the Lagrangian timescale.

[52] The final remark is that while Businger predicts a height-independent increase in eddy diffusivity for heavy particles, relative to the eddy viscosity, our results suggest a *reduction*, which is strongly height dependent.

7. Conclusions

[53] We have presented a one-dimensional stochastic model for heavy particle trajectories in turbulent boundary layer flow and applied it to the classic case of suspension of particles above an infinite flat plane. In the limit of small time steps, the model (with appropriate boundary conditions) is consistent with the well-mixed condition for non inertial, neutrally buoyant particles in the neutral surface layer, but neutrally buoyant inertial particles accumulate near the ground where the inertial timescale is long in comparison with the Lagrangian timescale (turbophoresis). For heavy inertial particles, our model results show departures from the power law concentration profile near the lower boundary, with increased particle concentrations close to the boundary, as with the neutral inertial particles. They also support *Xiao and Taylor*'s [2002] conclusion that particles with small gravitational settling cannot achieve steady state in finite time in an infinitely deep layer.

[54] Effective settling velocities are shown to be equal to w_s at large heights but are reduced significantly near the wall. Our model results suggest that, near the lower boundary, the effective eddy diffusivity for heavy particles is reduced in relation to the diffusion limit of the Langevin equation, and that the ratio K_f/K_m is significantly different from that predicted by *Businger* [1965].

[55] **Acknowledgments.** This work has been supported through grants from the Natural Sciences and Engineering Research Council of Canada in support of the MacKenzie GEWEX study. Joyce Kwan carried out some of the initial programming and testing of the IP model, and we are grateful to Tom Flesch for pointing out the relationship of our results to turbophoresis. A discussion with Joost Businger in the NCAR cafeteria initiated our study. Referee comments were very helpful in improving the presentation of our findings.

References

Budd, W. F., The drifting of nonuniform snow particles, in *Studies in Antarctic Meteorology*, *Antarc. Res. Ser.*, vol. 9, edited by M. J. Rubin, pp. 59–70, AGU, Washington, D. C., 1966.

Businger, J. A., Eddy diffusion and settling speed in blown snow, *J. Geophys. Res.*, *70*, 3307–3313, 1965.

Caporaloni, M., F. Tampieri, F. Trombetti, and O. Vittori, Transfer of particles in nonisotropic air turbulence, *J. Atmos. Sci.*, *32*, 565–568, 1975.

Csanady, G. T., Turbulent diffusion of heavy particles in the atmosphere, *J. Atmos. Sci.*, *20*, 201–208, 1963.

Devenish, B. J., D. C. Swailes, and Y. A. Sergeev, A PDF model for dispersed particles with inelastic particle-wall collisions, *Phys. Fluids*, *11*, 1858–1868, 1999.

Durbin, P. A., Comments on papers by Wilson et al. (1981) and Legg and Raupach (1982), *Boundary Layer Meteorol.*, *29*, 409–411, 1984.

Kind, R. J., Concentration and mass flux of particles in aeolian suspension near tailings deposal sites or similar sources, *J. Wind Eng. Ind. Aerodyn.*, *41–44*, 217–225, 1992.

Lees, B. L., Relationship between eddy viscosity of seawater and eddy diffusivity of suspended particles, *Geo Mar.*, *1*, 249–254, 1981.

Prandtl, L., *Essentials of Fluid Dynamics—With Applications to Hydraulics, Aeronautics, Meteorology and Other Subjects*, 425 pp., Blackie and Son, London, 1952.

Raupach, M. R., Diffusion of heavy particles in a turbulent flow, in *Heat and Mass Transfer in the Natural Environment: A Tribute to J. R. Philip*, *Geophys. Monogr. Ser.*, edited by D. E. Smiles, P. A. C. Raats, and A. W. Warrick, AGU, Washington, D. C., in press, 2002.

Reeks, M. W., The transport of discrete particles in inhomogeneous turbulence, *J. Aerosol. Sci.*, *14*, 729–739, 1983.

Rodean, H. C., *Stochastic Lagrangian Models of Turbulent Diffusion*, *AMS Meteorol. Monogr.*, vol. 26, no. 48, 84 pp., Am. Meteorol. Soc., Boston, Mass., 1996.

Sawford, B. L., Project Prairie Grass—A classic atmospheric dispersion experiment revisited, in *Proceedings of the 14th Australasian Fluid Mechanics Conference*, Univ. of Adelaide, Adelaide, South Australia, 2001.

Sawford, B. L., and F. M. Guest, Uniqueness and universality of Lagrangian stochastic models of turbulent dispersion, in *8th Symposium on Turbulence and Diffusion*, Am. Meteor. Soc., Boston, Mass., 1988.

Sawford, B. L., and F. M. Guest, Lagrangian statistical simulation of the turbulent motion of heavy particles, *Boundary Layer Meteorol.*, *54*, 147–166, 1991.

Shao, Y., *Physics and Modelling of Wind Erosion*, 393 pp., Kluwer Acad, Norwell, Mass., 2000.

Sommerfeld, R., and J. A. Businger, The density profile of blown snow, *J. Geophys. Res.*, *70*, 3303–3306, 1965.

Thomson, D. J., Criteria for the selection of stochastic models of particle trajectories in turbulent flows, *J. Fluid Mech.*, *180*, 529–556, 1987.

Wilson, J. D., Trajectory models for heavy particles in atmospheric turbulence: Comparison with observations, *J. Appl. Meteorol.*, *39*, 1894–1912, 2000.

Wilson, J. D., and T. K. Flesch, Flow boundaries in random-flight dispersion models: Enforcing the well-mixed condition, *J. Appl. Meteorol.*, *32*, 1695–1707, 1993.

Wilson, J. D., and B. L. Sawford, Review of Lagrangian stochastic models for trajectories in the turbulent atmosphere, *Boundary Layer Meteorol.*, *78*, 191–210, 1996.

Wilson, J. D., G. W. Thurtell, and G. E. Kidd, Numerical simulation of particle trajectories in inhomogeneous turbulence, III, Comparison of predictions with experimental data for the atmospheric surface layer, *Boundary Layer Meteorol.*, *21*, 443–463, 1981.

Xiao, J., and P. A. Taylor, On equilibrium profiles of suspended particles, *Boundary Layer Meteorol.*, *105*, 471–482, 2002.

P. Y. Li and P. A. Taylor, Department of Earth and Atmospheric Science, York University, 4700 Keele Street, Toronto, Ontario M3J 1P3, Canada. (mapyli@YorkU.CA; pat@YorkU.CA)

J. D. Wilson, Department of Earth and Atmospheric Sciences, University of Alberta, Edmonton, Alberta T6G 2E3, Canada. (jaydee.uu@ualberta.ca)